Differential Rotation of the Solar Chromosphere: A Century-long Perspective from Kodaikanal Solar Observatory Ca II K Data

Dibya Kirti Mishra [iD],[1,2] Srinjana Routh [iD],[1,2] Bibhuti Kumar Jha [iD],[3] Theodosios Chatzistergos [iD],[4] Judhajeet Basu [iD],[5] Subhamoy Chatterjee [iD],[3] Dipankar Banerjee [iD],[1,5,6] and Ilaria Ermolli [iD][7]

[1]*Aryabhatta Research Institute of Observational Sciences, Nainital-263002, Uttarakhand, India*
[2]*Mahatma Jyotiba Phule Rohilkhand University, Bareilly-243006, Uttar Pradesh, India*
[3]*Southwest Research Institute, Boulder, CO 80302, USA*
[4]*Max Planck Institute for Solar System Research, Justus-von-Liebig-Weg 3, D-37077 Göttingen,Germany*
[5]*Indian Institute of Astrophysics, Koramangala, Bangalore 560034, India*
[6]*Center of Excellence in Space Sciences India, IISER Kolkata, Mohanpur 741246, West Bengal, India*
[7]*INAF Osservatorio Astronomico di Roma, Via Frascati 33, 00078 Monte Porzio Catone, Italy*

ABSTRACT

Chromospheric differential rotation is a key component in comprehending the atmospheric coupling between the chromosphere and the photosphere at different phases of the solar cycle. In this study, we therefore utilize the newly calibrated multidecadal Ca II K spectroheliograms (1907–2007) from the Kodaikanal Solar Observatory (KoSO) to investigate the differential rotation of the solar chromosphere using the technique of image cross-correlation. Our analysis yields the chromospheric differential rotation rate $\Omega(\theta) = (14.61 \pm 0.04 - 2.18 \pm 0.37 \sin^2\theta - 1.10 \pm 0.61 \sin^4\theta)°/\text{day}$. These results suggest the chromospheric plages exhibit an equatorial rotation rate 1.59% faster than the photosphere when compared with the differential rotation rate measured using sunspots and also a smaller latitudinal gradient compared to the same. To compare our results to those from other observatories, we have applied our method on a small sample of Ca II K data from Rome, Meudon, and Mt. Wilson observatories, which support our findings from KoSO data. Additionally, we have not found any significant north-south asymmetry or any systematic variation in chromospheric differential rotation over the last century.

Keywords: The Sun (1693) — Solar atmosphere (1477) — Solar chromosphere (1479) — Plages (1240) — Solar cycle (1487) — Solar rotation (1524) — Solar differential rotation (1996)

1. INTRODUCTION

Solar rotation has been one of the persistent topics of interest in solar physics since its discovery at the beginning of the 17th century (Paternò 2010). Early investigations into this phenomenon were primarily based on the tracking of prominent dark photospheric magnetic features called sunspots (Carrington 1859; Newton & Nunn 1951), which enabled us to measure the photospheric differential rotation giving rise to the well-known empirical relation

$$\Omega = A + B\sin^2\theta + C\sin^4\theta, \qquad (1)$$

Corresponding author: Dipankar Banerjee
dipu@aries.res.in

where θ is the latitude, A is the equatorial rotation rate while B and C are coefficients of a quadratic expansion in $\sin^2\theta$. In the last century, there has been an outstanding advancement in instruments and measuring techniques, which not only improved the method of sunspot tracking (Newton & Nunn 1951; Ward 1966; Balthasar et al. 1986; Gupta et al. 1999; Javaraiah et al. 2005; Jha et al. 2021) but also led us to measure the solar rotation based on new techniques such as spectroscopy (Howard & Harvey 1970; Howard et al. 1984) and helioseismology (Komm et al. 2008; Howe 2009). As a result, in the last few decades, extensive research has been conducted in this field, leading to a consensus among researchers about the differential rotation profile of the Sun in both its interior and photosphere. Despite such extensive work, many questions still need to

be answered. One of many such prevailing questions is the variation in the rotational profile of the higher solar atmosphere, where the magnetic field mainly dominates the dynamics (Stix 1976; Gary 2001; Rodríguez Gómez et al. 2019).

Observations on spectral lines like Ca ɪɪ K centered at 393.367 nm, probe the chromospheric layer of the Sun (Linsky & Avrett 1970; Livingston et al. 2007), thus opening up new doors directed towards answering the question of chromospheric differential rotation. One of the predominantly visible features in the Ca ɪɪ K observations is the chromospheric plage, which is generally found above sunspots. These plages are the large-scale magnetic structures (Zirin 1974) having a relatively extended lifetime compared to the other features observed in Ca ɪɪ K observations. The extended lifetime and relatively stable nature of these plages make them an ideal candidate for measuring the chromospheric rotational profile (Singh & Prabhu 1985; Bertello et al. 2020).

Chromospheric plages are, however, extended structures (extend up to $\approx 200,000$ km; Priest 2014) compared to sunspots (up to $\approx 60,000$ km; Solanki 2003) that seem to change their morphology relatively faster when compared to the same. This makes tracer-based tracking algorithms, similar to the one used in, e.g. Newton & Nunn (1951), Jha et al. (2021) etc., unreliable for application. Having recognized this problem, Livingston (1969); Livingston & Duvall (1979) utilized Hα spectroscopic data for the chromosphere and reported a rotation rate $3\% - 8\%$ faster than the underlying photosphere. Despite the limitations of the tracer method, some have attempted to use it to investigate chromospheric differential rotation. Schroeter & Woehl (1975); Belvedere et al. (1977); Antonucci et al. (1979); Ternullo et al. (1987); Brajša et al. (1991) employed this approach by tracing the Ca ɪɪ network, plages, and polar filaments. The collective findings from these studies indicate that the chromosphere rotates $1\% - 5\%$ faster than the photosphere. Ternullo (1986) also reported variations in the rotation of plage with their age. In addition to these, recent studies conducted by Li et al. (2020); Xu et al. (2020), utilizing data in He ɪ and Mg ɪɪ lines, reported a faster rotation of the chromosphere. Subsequently, many have extended their observations to higher layers of the solar atmosphere (Brajša et al. 2004; Chandra et al. 2010; Li et al. 2019; Sharma et al. 2020; Zhang et al. 2023), and employed alternative methods, including the tracing of Coronal Bright Points (CBPs; Brajša et al. 2004; Hara 2009; Simon & Noyes 1972), as well as the Lomb-Scargle periodogram analysis (Li et al. 2019) and autocorrelation method (Chandra et al. 2010; Sharma et al. 2020; Zhang et al. 2023). The outcomes

from these studies also suggest the faster rotation of the higher solar atmosphere compared to the photosphere.

These results were contrasting those by Singh & Prabhu (1985), who employed the Fast Fourier Transform (FFT) method on Ca ɪɪ K plage area data (1951–1981) obtained at Kodaikanal Solar Observatory (KoSO) and concluded that the chromosphere exhibited a slower rotation compared to the photosphere. In a recent study, a different approach was employed to support this observation further. Bertello et al. (2020) employed the image cross-correlation technique, instead of FFT, on Ca ɪɪ K data acquired at Mount Wilson Observatory (MWO; 1915–1985) and found that the chromospheric plages give 0.63% slower rotation than the photospheric sunspots. Furthermore, studies comparing active regions in the photosphere and their counterparts in the chromosphere highlight their great spatial correspondence (e.g. Babcock & Babcock 1955; Loukitcheva et al. 2009; Chatzistergos et al. 2019; Murabito et al. 2023), which would suggest that there is no significant change in the rotational profile between photosphere and chromosphere.

The conflicting findings among these various studies pose a significant challenge in establishing a definitive understanding of the rotation profile of the chromosphere in relation to the underlying photosphere. Consequently, the question remains: Does the chromosphere rotate faster, slower, or in the same way as the photosphere? To gain deeper insights into the chromospheric rotation profile and its connection with the underlying photosphere, it is crucial to have a comprehensive and consistent dataset that minimizes biases caused by different aspects of solar activity, such as the phase and strength of the solar cycle. Fortunately, the Kodaikanal Solar Observatory (KoSO) possesses an extensive collection of Ca ɪɪ K archival data spanning over a century (1904–2007), obtained using the same setup throughout this period (Priyal et al. 2014; Jha 2022). These data have recently been re-calibrated by Chatzistergos et al. (2018, 2020), resulting in improved data quality. The availability of such long-term data presents a significant advantage, as it allows differential rotation measurement and temporal variation over the last century and helps us to resolve some of the questions about chromospheric rotation. This article presents an overview of the data and their processing in section 2. In section 3, we describe our approach to computing the differential rotation and present our results in section 4. Finally, we discuss our results and summarize our conclusions in section 5 and section 6.

2. DATA AND PROCESSING

The KoSO has a rich collection of Ca II K spectroheliograms taken on photographic plates/films, spanning over a century from 1904 to 2007 and is one of the oldest repositories of such data (Chatzistergos et al. 2022; Jha 2022). At KoSO, a spectroheliograph with a 30 cm objective lens and f/21 focal ratio was used for these observations. This spectroheliograph is fed by a siderostat, which compensates for the effect of the rotation of the Earth by keeping the reflected beam of sunlight in a fixed direction. Later, this reflected beam is passed through a diffraction grating system that allows Ca II K wavelength with a pass band of 0.05 nm centered at 393.367 nm (Bappu 1967; Jha 2022). In recent years, these photographic plates/films have been digitized using a 4096×4096 pixels CCD sensor, with a bit depth of 16-bit and made available to the wider scientific communities[1] (Priyal et al. 2014; Chatterjee et al. 2016).

There have been various studies analyzing the KoSO Ca II K data (e.g. Priyal et al. 2014; Chatterjee et al. 2016). However, a more accurate calibration method was recently developed by Chatzistergos et al. (2018) and applied to the KoSO Ca II K observations, resulting in an improved series of these data. A brief summary of the method implemented in Chatzistergos et al. (2018) is as follows. This calibration involves several steps, which are pre-processing, photometric calibration and limb-darkening compensation. The main part of the pre-processing is the detection and circularisation of the solar disk in the images. Then, the photometric calibration is performed by constructing the calibration curve for each image accomplished by comparing the observed quiet Sun center-to-limb variation with that from modern CCD-based observations. Finally, a limb-darkening correction is applied to obtain the contrast images with uniform intensity over the solar disc up to 0.99 of its radius. See Chatzistergos et al. (2018, 2019a,b, 2020) for the comprehensive details of all these processing steps. In addition to these calibration processes, a novel and precise method was developed by Jha (2022) to orient KoSO images accurately. We note that accurate knowledge of the observation time is needed to align the images correctly. However, the data from the KoSO was found to have the inconsistent time of observations, resulting in erroneous orientation. Jha (2022) successfully addressed these issues by resolving the inconsistencies in the time of observation of the images. Here, for the purposes of the current work, we utilized the recently calibrated (Chatzistergos et al. 2020) and correctly ori-

ented observations (Jha 2022) of Ca II K for the period of 1907–2007. We emphasise that the data obtained during the period of 1904–1906 are not used in this work due to the unavailability of the timestamp information for the mentioned period, which is required to correctly orient the images using the method given in Jha (2022). Representative examples of calibrated and orientation-corrected images are shown in Figure 1(a) and 1(b).

Besides the KoSO Ca II K data, we have also made use of a small sample of other Ca II K observations from a few relevant archives for comparison purposes. In particular, we used data from the Meudon (Malherbe & Dalmasse 2019), Mt Wilson (Bertello et al. 2020), and Rome (taken with the Rome Precision Solar Photometric Telescope, Rome/PSPT; Ermolli et al. 2022) datasets. Meudon is one of the oldest Ca II K archives, with observations since 1893 and continues to this day after some modifications in the instrumentation (Malherbe 2023). These were photographic observations stored on glass plates up to 27 September 2002, while observations with a CCD camera started on 13 May 2002, and they were performed with a spectroheliograph with a nominal pass band of 0.015nm (Malherbe & Dalmasse 2019). Mt Wilson also comprises spectroheliograms covering the period 1915–1985 with a nominal pass band of 0.035 nm (Tlatov et al. 2009). Rome/PSPT has observations from 1996 up to the present. It uses a CCD camera and an interference filter with a bandwidth of 0.25nm (Ermolli et al. 2022). In particular, we used 829 and 569 images from Meudon and Rome/PSPT, respectively, over the period of $2000-2002$, which is close to the solar maximum of cycle 23 and 408 images from Mt Wilson over the period 1978–1979, in the ascending phase of cycle 21. The images were processed with the same methods as KoSO to compensate for the limb darkening and perform the photometric calibration for the photographic data from Meudon and Mt Wilson (Chatzistergos et al. 2018, 2019a, 2020).

Finally, for comparison purposes, we also used Mt Wilson data over the period 1978–1979 processed by Bertello et al. (2010)[2], as well as raw (without processing to compensate the limb-darkening or perform the photometric calibration) Mt Wilson data. For the raw data, we further used two different versions; the first one is with the preprocessing (definition of center coordinates and image rotation) by Bertello et al. (2010) and the second one by Chatzistergos et al. (2020). The latter case applied a correction for the recorded solar disk

---

[1] The digitized data can be accessed through https://kso.iiap.res.in/data.

[2] Available at ftp://howard.astro.ucla.edu/pub/obs/CaK/run_mean_flat/

elliptity, thus accounting for the image distortions (see Chatzistergos et al. 2020; Chatzistergos et al. 2020).

3. METHODOLOGY

Considering the relatively dynamic and spatially extended nature of the plage region in Ca II K observations, in this work, we used the image cross-correlation-based technique to quantify the chromospheric differential rotation rate. We start with selecting a pair of observations, preferably consecutive, but in such a way that the difference in observation time (Δt) of the selected observation is more than 0.5 days but less than 1.5 days. This lower limit on Δt is imposed to eliminate the effects of other rapidly evolving features (having a life span less than 0.5 days) and the upper limit to minimize the effects of the evolution of plages. Furthermore, these limits have also been used to ensure that one image per day will be selected, which is close to the average cadence of the KoSO digital archive.

Firstly, we project the selected pair of full disk observations, shown in Figure 1(a) and 1(b), to the heliographic grid (Thompson 2006) of size 1800 pixels $\times$ 1800 pixels (0.1°/pixel in latitude and longitude) as shown in Figure 1(c) and (d), using the near-point interpolation method. While projecting the full disk observation on the heliographic grid, we restricted ourselves to the inner 0.98 $R_\odot$ (shown by the red line in Figure 1(a) and (b)) to avoid the significant distortion near the limbs caused by the projection effects. Here, we have not reduced the dimension of the image but only analysed the disk up to 0.98 $R_\odot$. Then, we split the image in 5° latitudinal bands (see red rectangular boxes and zoomed-in view shown in insets in Figure 1 B1 and B2). We restrict ourselves between $\pm 55°$ in latitude and longitude to further minimize the effect of projection near the limb and also because plages are very unlikely to appear above these latitudes. Following this, we apply the 2D image cross-correlation technique within the 5° latitudinal bands to get the magnitude of the spatial movement of the features (here, plages). The steps of image cross-correlations are described as follows.

To reduce the computational time, we start with the initial guess [$\Delta\phi_0$ and $\Delta\theta_0$] that presumably gives the best correlation coefficient. The $\Delta\phi_0$ is calculated based on the photospheric rotation rate measured from the KoSO White Light (WL) data (Jha et al. 2021) for the selected band using $\Delta\phi_0 = \Omega(\theta)\Delta t$, where $\Omega(\theta)$ is the angular rotation rate at latitude θ (taken as the mid-latitude of the selected band). Assuming that the plages do not show considerable movement in the meridional plane, $\Delta\theta_0$ is taken as 0. We then calculate the stan-
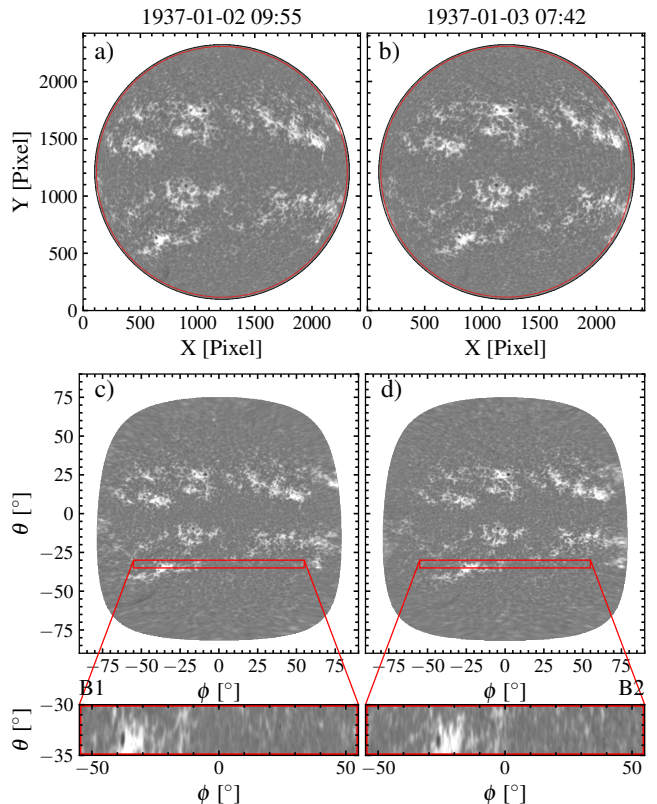

Figure 1. Example pair of calibrated and rotation-corrected full disk Ca II K images from KoSO as recorded on (a) 1937-01-02 09:55 IST and (b) 1937-01-03 07:42 IST. The red dotted circles represent the 0.98 $R_\odot$ limit. Panels (c) and (d) show the corresponding full disk images projected on the heliographic grid. Red rectangular boxes in (c) and (d) represent the selected latitude bands (in this case $-35°$ to $-30°$) for the cross-correlation. Zoomed-in views of the bands are shown in the inset (B1 and B2).

dard 2D cross-correlation (CC)[3] for each 0.1° shift in the range of [$\Delta\phi_0 \pm 2°$, $\Delta\theta_0 \pm 1°$]. In Figure 2, we plot the correlation matrix for all the combinations of shifts for B1 and B2 in physical units ($\Delta\theta$ and $\Delta\phi$, i.e., shift in latitude and longitude) by adjusting it for the initial offset of [$\Delta\phi_0$, $\Delta\theta_0$], for the better interpretation. Consequently, we calculate the optimum shift ($\Delta\theta$ and $\Delta\phi$) for which the CC value is maximum (represented by the small red dot in Figure 2a). In Figure 2(b) and (c), we also show the variation of CC with $\Delta\phi$ for fixed $\Delta\theta$ and with $\Delta\theta$ for fixed $\Delta\phi$, respectively. We repeat this process for all latitude bands in the range of $\pm 55°$

---

[3] The image cross-correlation was performed using correl_images.pro routine available in the Solar SoftWare library. For detail see https://hesperia.gsfc.nasa.gov/ssw/gen/idl_libs/astron/image/correl_images.pro.

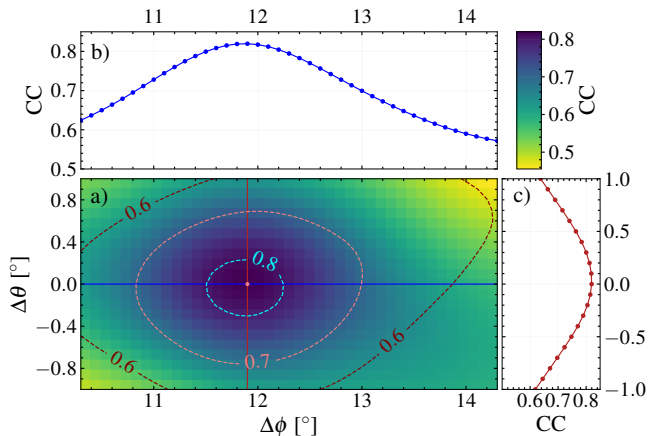latitude and for all the pairs of observations from the period 1907–2007.

Figure 2. (a) Variation of the correlation coefficient for all the combinations of longitudinal ($\Delta\phi$) and latitudinal ($\Delta\theta$) shifts. The red dot represents the point of maximum CC (CC_{max}), and the contours show the lines of constant CC. (b) and (c) show the variation of CC with $\Delta\phi$ for constant $\Delta\theta$ (along blue horizontal line) and, $\Delta\theta$ for constant $\Delta\phi$ (along red vertical line), for $\Delta\phi$ and $\Delta\theta$ corresponding to the location of maximum CC.

We find for $\approx 50\%$ of cases ($\approx 66\%$ and $\approx 42\%$ for $\theta < 20$ and $\theta > 20$ respectively), considering all the latitude bands, the maximum correlation coefficient (CC_{max}) lies in the range [0.2, 0.8]. Additionally, We have also encountered cases where (i) CC_{max} is less than 0.2 and (ii) no local maximum (CC_{max}) is found, i.e., either it lies at the extreme ends or no/minute variation in CC in the given shift ranges (one such case is shown in Figure 8 from Appendix A). In Figure 3, we show the cumulative distribution of the CC_{max} for the Northern and Southern hemispheres in two latitude ranges (i) $\theta \leq 20°$ and (ii) $\theta > 20°$, depicting the fraction of CC_{max} in various ranges. Furthermore, we also looked at the change in differential rotation parameter by changing the lower limit of CC_{max} (see Appendix A), and we note that there is no significant change in rotation parameters after $CC_{max}=0.2$. Hence, considering the potential negative impact of cases where $CC_{max} < 0.2$, they are discarded from our analysis.

After discarding the cases mentioned above, we calculate the synodic rotation rate ($\Omega_{synodic}$) using the $\Delta\phi$ corresponding to the CC_{max} and Δt as

$$\Omega_{synodic} = \frac{\Delta\phi}{\Delta t}. \qquad (2)$$

To incorporate the effect of the motion of the Earth around the Sun, we apply a correction on the synodic rotation rate to get the sidereal rotation rate using the
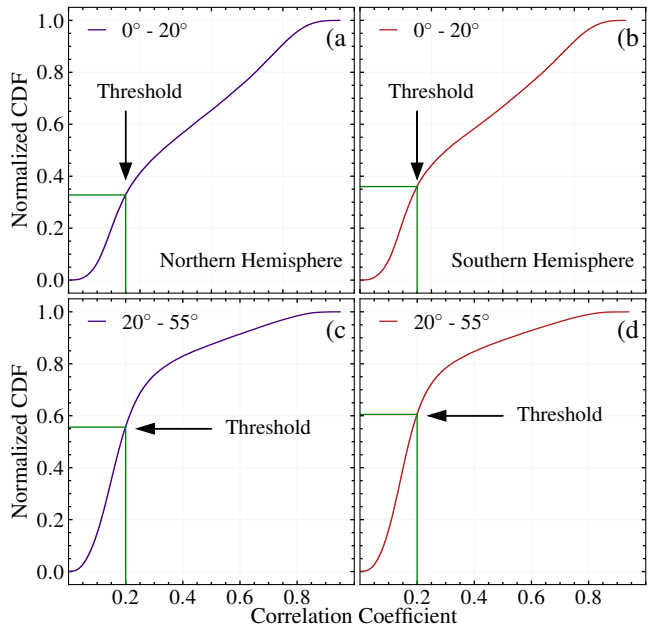

Figure 3. The normalized cumulative distribution of CC_{max} for the Northern hemisphere for latitude range (a) $\theta \leq 20°$ and (b) $\theta > 20°$. A similar plot for the Southern hemisphere is shown in (b) and (d). The arrow in each panel highlights the lower threshold limit of CC_{max} which is 0.2, used in our analysis.

relation (Roša et al. 1995; Wittmann 1996; Skokić et al. 2014)

$$\Omega_{sidereal} = \Omega_{synodic} + \frac{\overline{\Omega}_{Earth}}{r^2} \left(\frac{\cos^2 \psi}{\cos i} \right), \qquad (3)$$

where $\overline{\Omega}_{Earth}$ is the mean orbital angular velocity of the Earth (0.9856 °/day), i is the inclination of the solar equator to the ecliptic, ψ is the angle between the pole of the ecliptic and the solar rotation axis orthographically projected on the solar disk, and r is the Sun-Earth distance in Astronomical Units (AU; Lamb 2017; Jha et al. 2021). Hereafter, we drop the subscript sidereal from $\Omega_{sidereal}$ and use Ω instead for the same.

4. RESULTS

4.1. *Average Chromospheric Rotation Profile*

To get the latitudinal variation of the rotation profile, we calculate the mean of Ω for each latitude band. These mean Ω are shown by the filled red circles in Figure 4(a) as a function of latitude (θ). We performed two error estimations for our calculations: (i) the least count error (σ_{LCE}) due to the resolution of the heliographic grid, i.e. $0.1/\Delta t$ ($\Delta\phi$ will have at least 0.1° uncertainty) and (ii) the standard statistical error (σ_{SSE}) of the mean. We calculate the combined errors in our analysis by the relation $\sigma_{total} = \sqrt{(\sigma_{LCE})^2 + (\sigma_{SSE})^2}$. However, σ_{LCE} is

dominant in the total error estimation, as σ_{LCE} is an order of magnitude greater than the σ_{SSE}. Therefore, we find approximately the same errors (light red continuous band in Figure 4(a) in all latitude bands. Now, we fit Equation 1 to the mean Ω obtained using the Levenberg-Marquardt least square (LMLS; Markwardt 2009) fitting method to get the differential rotation parameters A, B and C (see Table 1). The very first thing that we note is that our results suggest that the chromosphere plages give rotation rate $\approx 1.59\%$ faster than the underlying photosphere, as inferred by using WL sunspot data (blue dashed line in Figure 4(a); Jha et al. 2021), which is in disagreement with the chromospheric rotation rate obtained in Bertello et al. (brown dashed-dotted in Figure 4(b); 2020) using MWO Ca II K data. Interestingly, a very recent work (Li et al. 2023) reports a faster-rotating chromosphere using the auto-correlation technique on Ca II K synoptic maps from MWO. We will discuss more about the possible reasons behind this discrepancy as seen from MWO Ca II K plage data in section 5.

We also observed a relatively higher rotation rate from the average value in the 2nd half period of KoSO data. As can be seen in Figure 4(a) and Table 1, the rotation rate averaged after 1980 (purple curve) is higher than the rotation rate averaged before 1980 (green curve) as well as the total average rotation profile (1907–2007; red curve). We suspect this may be due to the degraded data quality after 1980, as reported by Chatterjee et al. (2016); Priyal et al. (2014); Chatzistergos et al. (2019b).

There are two other works that attempt to measure the chromospheric rotation rate, Antonucci et al. (1979) and Wan & Li (2022), using Ca network and Ca II K filaments, respectively, suggesting faster rotation of the chromosphere. These chromosphere rotation rates obtained in the past are overplotted in Figure 4(b) to show a comparison with the rotation rate of the photosphere, measured by tracking sunspots (Jha et al. 2021) and spectroscopic method (Howard et al. 1983). Except Bertello et al. (2020) obtained from MWO data, all other results suggest that the chromospheric plages (and other chromospheric features) give a faster rotation rate than the photospheric rotation rate obtained from sunspot or surface rotation rate measured using spectroscopic methods.

To further investigate these slightly different results obtained in the measured rotation rate, we implemented our image cross-correlation-based differential rotation measurement technique to the small sample of other data sets, which are discussed in the following section.

4.2. Comparison with Other Observatories

To test the robustness of our algorithm and to ensure that the result that we are getting is not an artefact of the data, we implemented it on the Ca II K data obtained at Meudon (Malherbe & Dalmasse 2019) and Rome/PSPT (Ermolli et al. 1998, 2022) for the period of $2000-2002$, which is close to the solar maximum and have significant plage regions. We applied the same process to determine the chromospheric rotation in the Meudon and Rome/PSPT data as we did for the KoSO ones. In Figure 4(c), we compare our results for the chromospheric rotation rate from KoSO, Meudon, and Rome/PSPT by using data only over the period $2000-2002$. We find all three Ca II K datasets to result in differential rotations that are indeed faster than the one found for the photosphere by tracing sunspots (Jha et al. 2021). Additionally, it is crucial to acknowledge that, although the central wavelength of Ca II K filter for all these observatories is the same, they have different pass bands, e.g., KoSO: 0.05 nm (Priyal et al. 2014), Meudon: 0.015 nm (Malherbe & Dalmasse 2019), and Rome/PSPT: 0.25 nm (Ermolli et al. 1998, 2022). Furthermore, KoSO and MWO data are spectroheliograms, while Rome/PSPT are filtergrams; thus, the shape of the pass bands might also differ. Consequently, these data sets have contributions from slightly different layers of the chromosphere, and this might play a role in the differences observed in the results. In Table 2, we outline the differential rotation parameters from the best fit (Equation 1) for all these cases using the data over the period $2000-2002$. However, we do not observe a monotonic change in differential rotation with archive bandwidth, thus height in the solar atmosphere. Furthermore, in Table 2, we also note that the rotation rate obtained from the KoSO Ca II K data is relatively higher than the average rotation rate obtained from the same over the entire span of data (Table 1). The reason behind this observed higher value is already discussed in subsection 4.1. We further extended the test of the robustness of our algorithm by implementing it on Michelson Doppler Imager (MDI; Scherrer et al. 1995) intensity continuum data and MWO Ca II K data (discussed in Appendix B) to compare with the already obtained results in Jha et al. (2021) and Bertello et al. (2020), respectively.

4.3. North-South Asymmetry

There are various works (Schroeter & Woehl 1975; Livingston & Duvall 1979; Wan et al. 2023) that suggest that the chromosphere shows a significant difference in the observed rotation rate in the Northern and Southern hemispheres. Therefore, firstly, to investigate the
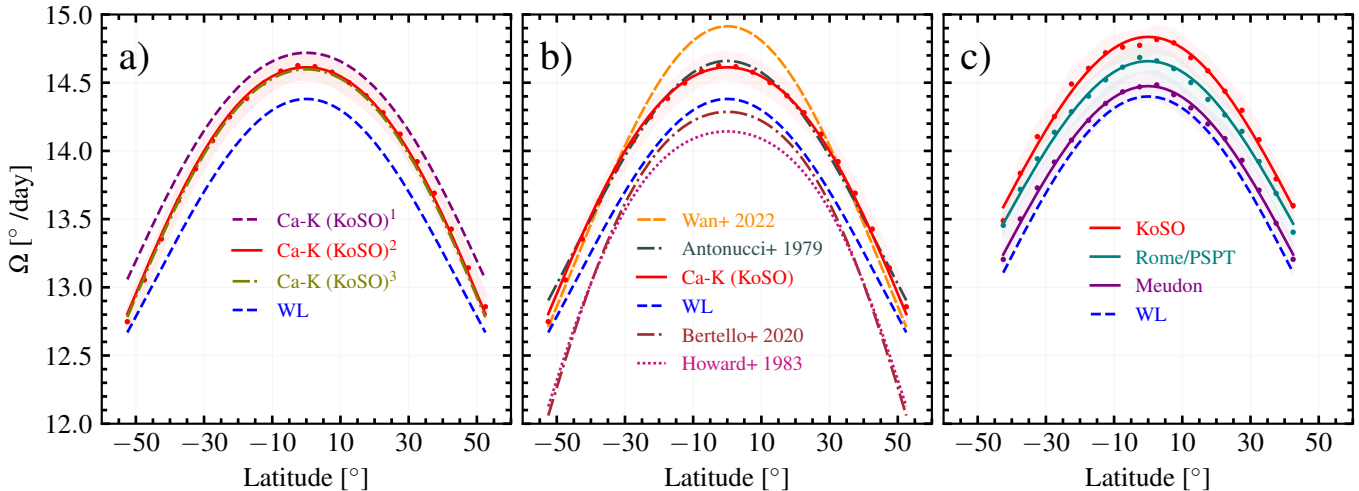
Figure 4. a) The average rotation rate of the entire data period (1907–2007) calculated in each latitude band as a function of latitude along with the best-fit curve to the observed data represented as a solid red curve in the latitude range of $\pm 55°$. Dashed blue is the rotation profile of the photosphere using sunspot (Jha et al. 2021). The purple and olive curves are for the chromosphere rotation profile using KoSO data for two different periods: 1980–2007 and 1907–1979, respectively. b) Comparison between our results for KoSO data for the entire period and selected works from the literature. c) A comparison between the resulting rotation profile of the chromosphere derived from different sources of Ca II K data over 2000–2002. In particular, we show results for KoSO (red), Rome/PSPT (teal), and Meudon (purple) Ca II K data. The dashed blue curve shows the rotation profile of the photosphere over the same period.
Note - $^1 = (1980–2007)$, $^2 = (1907–2007)$, $^3 = (1907–1979)$

Table 1.   Solar differential rotation parameters from different observations

Study	Data/Features	Observatory	Period	$A \pm \Delta A$	$B \pm \Delta B$	$C \pm \Delta C$
				($°$/day)	($°$/day)	($°$/day)
Howard et al. (1983)	Doppler Measurement	MWO	1967–1982	14.143 ± 0.006	-1.718 ± 0.005	-2.361 ± 0.007
Jha et al. (2021)	WL	KoSO	1923–2011	14.381 ± 0.004	-2.72 ± 0.04	—
Bertello et al. (2020)	Ca II K plage	MWO	1915–1985	14.2867 ± 0.0025	-2.128 ± 0.0351	-2.24 ± 0.0787
Wan & Gao (2022)	Ca II K plage	MWO	1915–1985	13.496 ± 0.084	-2.468 ± 0.656	—
Antonucci et al. (1979)	Ca II K Network	Anacapri	1972 (8 May–14 August)	14.66	-2.79	—
Wan & Li (2022)	Ca II K Filaments	Coimbra	1929–1941	14.914 ± 0.263	-3.505 ± 0.684	—
This work	Ca II K plage	KoSO	1907–2007	14.61 ± 0.04	-2.18 ± 0.37	-1.10 ± 0.61
This work	Ca II K plage	KoSO	1907–1979	14.59 ± 0.04	-2.23 ± 0.37	-1.05 ± 0.60
This work	Ca II K plage	KoSO	1980–2007	14.72 ± 0.04	-2.05 ± 0.39	-0.94 ± 0.64

NOTE—Columns are the bibliographic entry, type of observation and feature used, name of observatory, period covered by data, and the parameters of fitting Eq. 1.

North-South asymmetry in chromospheric rotation, we add the odd powers of $\sin \theta$ in Equation 1

$$\Omega = A + B' \sin \theta + B \sin^2 \theta + C' \sin^3 \theta + C \sin^4 \theta. \quad (4)$$

and again, fit this equation to the data using the LMLS method. Secondly, we use the Equation 1 and fit it individually in the Northern and Southern hemispheres. In Figure 6, we show all these three cases along with the fit of Equation 1 in both hemispheres. When we fit the asymmetric profile (Equation 4), we note that the odd-order terms are very close to zero. Therefore,

we can safely say that there is no or significantly less contribution from these terms in the chromospheric rotation profile, and it is symmetric within our precision of measurement. This is also confirmed by fitting Equation 1 one by one in both hemispheres. The best fitting parameters are also summarized in Table 3.

We further investigate the difference in rotation rate in the Northern and Southern hemispheres by calculating the variation in rotation profile over the mean calculated from the entire duration of the data. Which we call a
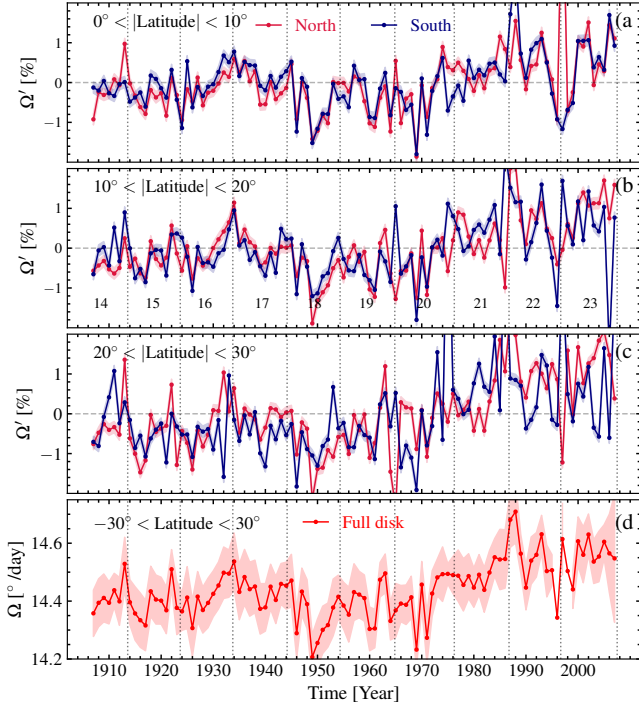
Figure 5. Relative variations (%) in rotation rate (Ω') in three different latitude bands (a) $0° - 10°$, (b) $10° - 20°$ and (c) $20° - 30°$ for the Northern and Southern hemispheres and variation of Ω (°/day) for the years of 1907–2007 in panel (d).
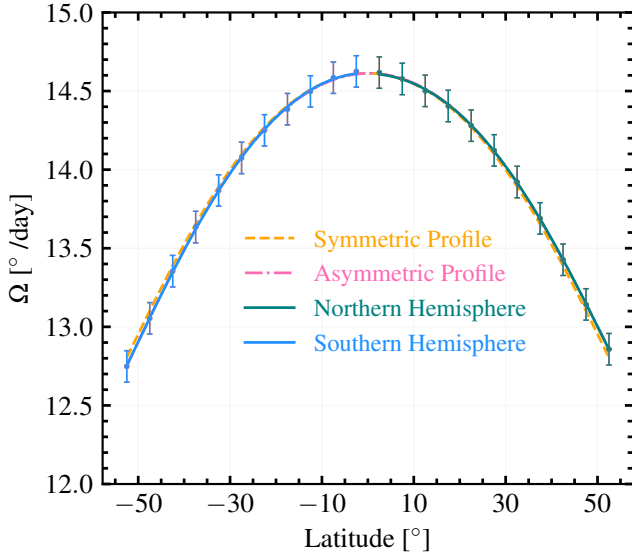

Figure 6. The best-fit lines for the case of asymmetric fitting (Equation 4) in both hemispheres together (pink) as well as symmetric fitting (Equation 1) in both hemispheres together (yellow) and independently in Northern and Southern hemispheres (teal and dodgerblue, respectively).

Table 2. Comparison between our results for the differential rotation from KoSO, Rome/PSPT, and Meudon Ca II K data to those from KoSO WL data by Jha et al. (2021) for the period 2000–2002.

Data	$A \pm \Delta A$ (°/day)	$B \pm \Delta B$ (°/day)	$C \pm \Delta C$ (°/day)
KoSO[1]	14.39	-2.83	—
KoSO[2]	14.80 ± 0.05	-2.13 ± 0.56	-1.39 ± 1.25
Rome/PSPT[2]	14.64 ± 0.05	-2.31 ± 0.57	-0.68 ± 1.24
Meudon[2]	14.46 ± 0.04	-2.39 ± 0.56	-0.71 ± 1.22

NOTE—[1] Jha et al. (2021) for WL data; [2] This study Ca II K data

relative change in rotation rate and define as

$$\Omega' = \frac{(\overline{\Omega}_{\text{year}} - \overline{\Omega}_{\text{all}})}{\overline{\Omega}_{\text{all}}} \times 100\%, \qquad (5)$$

where $\overline{\Omega}_{\text{year}}$ is the mean value over a year and $\overline{\Omega}_{\text{all}}$ is the mean value over the entire period 1907–2007. In Figure 5(a, b, c) we show the variation of Ω' in three different bands (i) $0° - 10°$, (ii) $10° - 20°$, and (iii) $20° - 30°$ for the Northern and the Southern hemispheres separately. We do note an upward trend in the rotation rate after 1980, consistent with the higher rotation rate obtained in Figure 4(c), which is again the consequence of the degraded data quality in these periods (see, e.g. Ermolli et al. 2009; Chatzistergos et al. 2023). Additionally, we also note this upward trend in Figure 5(d) after 1980 in the yearly averaged Ω, calculated by averaging over the disk (latitude range $-30°$ to $+30°$). Hence, the inference needs to be drawn very carefully.

5. DISCUSSION

One of the important aspects of the results obtained in this work is their dependence on various data sets, methods and calibration techniques. The results obtained based on the KoSO data are in contrast to Bertello et al. (2020) based on MWO Ca II K observations; at the same time, they are in agreement with the findings of Antonucci et al. (1979); Li et al. (2020); Wan & Li (2022). We speculate that the difference in the results may be attributed to the differences in the applied processing of the images as well as the pass bands of the filters utilized at the respective observatories, leading to a dataset-specific dependence of the results. However, we must highlight that our understanding of such a dependence remains incomplete. Recently, Li et al. (2023) utilized data from the MWO processed by Bertello et al. (2020) to arrive at a similar result to ours, thus contrasting that of Bertello et al. (2020), which further underlines the complexity in the pursuit of a complete understanding of

Table 3. Comparison between the differential rotation parameters of Eq. 4 for the Northern and Southern hemispheres.

Results	$A \pm \Delta A$	$B' \pm \Delta B'$	$B \pm \Delta B$	$C' \pm \Delta C'$	$C \pm \Delta C$
	(°/day)	(°/day)	(°/day)	(°/day)	(°/day)
Symmetric full disk	14.61 ± 0.04	—	-2.18 ± 0.37	—	-1.10 ± 0.61
Asymmetric full disk	14.61 ± 0.04	0.02 ± 0.11	-2.18 ± 0.38	0.07 ± 0.26	-1.10 ± 0.61
Symmetric Northern	14.61 ± 0.06	—	-2.07 ± 0.53	—	-1.14 ± 0.86
Symmetric Southern	14.62 ± 0.06	—	-2.29 ± 0.53	—	-1.06 ± 0.85

Note—As symmetric fit we refer to Eq. 1, while as asymmetric to Eq. 4.

such a dependence. We extended our analysis by applying our method of differential rotation measurement on MWO data calibrated by two different techniques: one is done by Bertello et al. (2010) and the other is done recently by Chatzistergos et al. (2020). Here we note that we used full disk Ca II K observations processed by Bertello et al. (2010) and not by Bertello et al. (2020), on one hand because Bertello et al. (2020) provides only Carrington maps while Bertello et al. (2010) gave the full disk images and on the other hand because the image processing applied in these two studies is effectively the same. Interestingly, we found a significant difference in our results (Figure 10c, d) for these two data sets, which indicated that the different approaches of image processing might lead to different and even contradictory results. Differences in how the two processing approaches account for image distortions and the ellipticity of the recorded solar disk were found to contribute to this, but they are not the dominant factor (compare yellow and pink curves in Fig. 7). Residual artifacts in the images or issues with their orientation can also affect the efficacy of the process of estimating the rotation rate. In this direction, how the different calibration steps affect the results can also be seen in Figure 7. Here, we note that the curves listed as "without DC" (pink) and "Without Calibration (WC)" (red) are the datasets of raw images that were used by Chatzistergos et al. (2020) and Bertello et al. (2010), respectively. Both datasets include MWO images without compensation for the limb darkening or circularisation of the solar disk; however, they differ in their spatial resolution (pink has the full resolution images, while red is for the reduced size images used by Bertello et al. 2010). Further differences exist because corrections in date/time information, as well as the orientation of the solar disk, were applied for the "without DC" curve compared to the "Without Calibration (WC)" one. This highlights the added uncertainty in the estimation of the differential rotation due to the spatial resolution and orientation of the images. However, the exact reason behind the differences is still veiled to us, and this would require a more in-depth analysis.

6. SUMMARY AND CONCLUSION

We use full disk Ca II K (393.367 nm) spectroheliograms from KoSO spanning a century (1907 – 2007; Cycles 14 to 23) to calculate the chromospheric differential rotation using a newly developed automatic algorithm. Our findings show that the average chromospheric rotation profile is

$$\Omega(\theta) = (14.61 - 2.18\sin^2\theta - 1.10\sin^4\theta)^\circ/\text{day} \quad (6)$$

which is ≈1.59% faster when compared with the photospheric equatorial rotation rate obtained by Jha et al. (2021) using WL KoSO data and ≈ 3.3% compared to the results by Howard et al. (1983) using MWO Doppler measurements (Figure 4(b), Table 1).

Our analysis supplements previous results (e.g. Livingston 1969; Antonucci et al. 1979; Li et al. 2020; Wan & Li 2022) suggesting that the higher layers of the solar atmosphere rotate faster than those underneath. We have validated our results by extending our method on the small samples of Ca II K data from other observatories such as Meudon, Rome/PSPT and MWO. Results obtained from these datasets extend affirmative support to our method as well as increase the reliability of our results. The contradiction of our result with that of Bertello et al. (2020), as well as the contradiction between results obtained using two distinctly different methodologies (Bertello et al. 2010; Chatzistergos et al. 2020), indicates a significant influence of image processing techniques as well as data-set specific factors. However, we must reiterate that the full extent of such an influence remains outside the scope of the current study.

In the past, based on these results, there have been attempts, such as that in Weber (1969), to explain the observed increase in rotation rate with height based on the conservation of angular momentum in a magnetic field-dominated medium. However, it is important to acknowledge our constrained understanding of the matter, which further underlines a need for careful measurements of the rotation rate farther in the solar atmosphere at various heights above the photosphere. Therefore, in a follow-up study, we are attempting to achieve the same by measuring the solar rotation rate
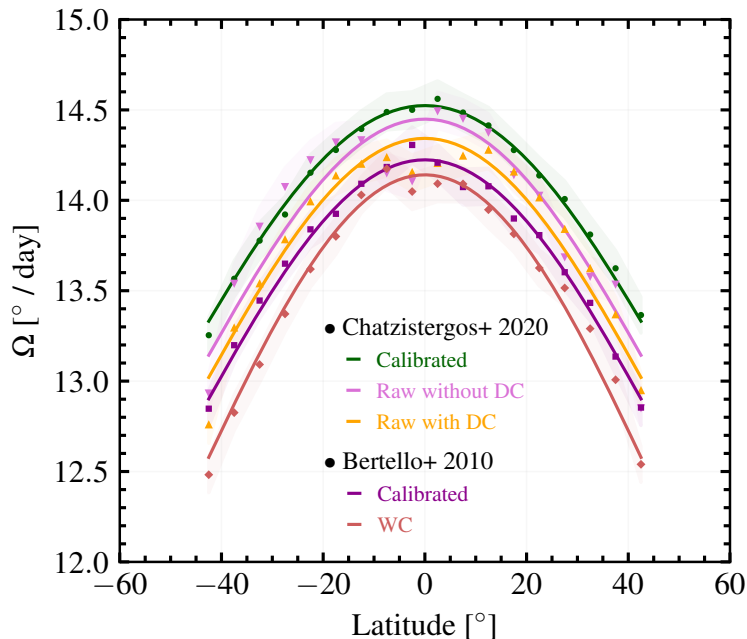
Figure 7. Comparison of differential rotation profiles derived with different levels of processing of MWO Ca ɪɪ K data over 1978–1979. The dark green and dark magenta curves show the rotation profiles using MWO data calibrated by Chatzistergos et al. (2020) and Bertello et al. (2010), respectively. The other three curves show raw scanned images without any processing to compensate for the limb darkening. The yellow and pink curves are for the raw images used by Chatzistergos et al. (2020) after applying the Disk Circularisation (DC) and without it, respectively. The red curve is for images Without Calibration (WC) used by Bertello et al. (2010). We note that the pink and red curves refer to data that differ in their spatial resolution (full size for pink, reduced size for red), have identified the solar disk differently, as well as differ in corrections that they applied in date/time and rotation angle.

even higher in the atmosphere. We hope such a study will complement the current work and help us advance the broader understanding of the solar atmosphere.

REFERENCES

Antonucci, E., Azzarelli, L., Casalini, P., Cerri, S., & Denoth, F. 1979, SoPh, 63, 17, doi: 10.1007/BF00155691

Babcock, H. W., & Babcock, H. D. 1955, The Astrophysical Journal, 121, 349, doi: 10.1086/145994

Balthasar, H., Vazquez, M., & Woehl, H. 1986, A&A, 155, 87

Bappu, M. K. V. 1967, SoPh, 1, 151, doi: 10.1007/BF00150312

Belvedere, G., Godoli, G., Motta, S., Paterno, L., & Zappala, R. A. 1977, ApJL, 214, L91, doi: 10.1086/182449

Bertello, L., Pevtsov, A. A., & Ulrich, R. K. 2020, ApJ, 897, 181, doi: 10.3847/1538-4357/ab9746

Bertello, L., Ulrich, R. K., & Boyden, J. E. 2010, SoPh, 264, 31, doi: 10.1007/s11207-010-9570-z

Brajša, R., Vršnak, B., Ruždjak, V., et al. 1991, SoPh, 133, 195, doi: 10.1007/BF00149885

Brajša, R., Wöhl, H., Vršnak, B., et al. 2004, Astronomy and Astrophysics, 414, 707, doi: 10.1051/0004-6361:20034082

Carrington, R. C. 1859, MNRAS, 19, 81, doi: 10.1093/mnras/19.3.81

Chandra, S., Vats, H. O., & Iyer, K. N. 2010, Monthly Notices of the Royal Astronomical Society, 407, 1108, doi: 10.1111/J.1365-2966.2010.16947.X

Chatterjee, S., Banerjee, D., & Ravindra, B. 2016, ApJ, 827, 87, doi: 10.3847/0004-637X/827/1/87

Chatzistergos, T., Ermolli, I., Krivova, N. A., & Solanki, S. K. 2019a, A&A, 625, A69, doi: 10.1051/0004-6361/201834402

Chatzistergos, T., Ermolli, I., Krivova, N. A., & Solanki, S. K. 2020, Journal of Physics: Conference Series, 1548, 012007, doi: 10.1088/1742-6596/1548/1/012007

Chatzistergos, T., Ermolli, I., Solanki, S. K., & Krivova, N. A. 2018, A&A, 609, A92, doi: 10.1051/0004-6361/201731511

Chatzistergos, T., Ermolli, I., Solanki, S. K., et al. 2019b, SoPh, 294, 145, doi: 10.1007/s11207-019-1532-5

Chatzistergos, T., Ermolli, Ilaria, Solanki, Sami K., et al. 2019, Astronomy & Astrophysics, 626, A114, doi: 10.1051/0004-6361/201935131

Chatzistergos, T., Krivova, N. A., & Ermolli, I. 2022, Frontiers in Astronomy and Space Sciences, 9, doi: 10.3389/fspas.2022.1038949

Chatzistergos, T., Ermolli, I., Krivova, N. A., et al. 2020, Astronomy & Astrophysics, 639, A88, doi: 10.1051/0004-6361/202037746

Chatzistergos, T., Ermolli, I., Banerjee, D., et al. 2023, Astronomy & Astrophysics, in press, doi: 10.1051/0004-6361/202347536

Ermolli, I., Fofi, M., Bernacchia, C., et al. 1998, Solar Physics, 177, 1

Ermolli, I., Giorgi, F., & Chatzistergos, T. 2022, Frontiers in Astronomy and Space Sciences, 9, doi: 10.3389/fspas.2022.1042740

Ermolli, I., Solanki, S. K., Tlatov, A. G., et al. 2009, ApJ, 698, 1000, doi: 10.1088/0004-637X/698/2/1000

Gary, G. A. 2001, SoPh, 203, 71, doi: 10.1023/A:1012722021820

Gupta, S. S., Sivaraman, K. R., & Howard, R. F. 1999, SoPh, 188, 225, doi: 10.1023/A:1005229124554

Hara, H. 2009, The Astrophysical Journal, 697, 980

Howard, R., Adkins, J. M., Boyden, J. E., et al. 1983, SoPh, 83, 321, doi: 10.1007/BF00148283

Howard, R., Gilman, P. I., & Gilman, P. A. 1984, ApJ, 283, 373, doi: 10.1086/162315

Howard, R., & Harvey, J. 1970, Solar Physics 1970 12:1, 12, 23, doi: 10.1007/BF02276562

Howe, R. 2009, SoPh, 6, 1, doi: https://doi.org/10.12942/lrsp-2009-1

Javaraiah, J., Bertello, L., & Ulrich, R. K. 2005, SoPh, 232, 25, doi: 10.1007/s11207-005-8776-y

Jha, B. K. 2022, PhD thesis, Department of Physics, Pondicherry University, doi: 10.48550/arXiv.2210.09072

Jha, B. K., Priyadarshi, A., Mandal, S., Chatterjee, S., & Banerjee, D. 2021, SoPh, 296, 25, doi: 10.1007/s11207-021-01767-8

Komm, R., Howe, R., Hill, F., & Hernández, I. G. 2008, Solar Physics 2008 254:1, 254, 1, doi: 10.1007/S11207-008-9285-6

Lamb, D. A. 2017, ApJ, 836, 10, doi: 10.3847/1538-4357/836/1/10

Li, K. J., Wan, M., & Feng, W. 2023, MNRAS, 520, 5928, doi: 10.1093/mnras/stad478

Li, K. J., Xu, J. C., Xie, J. L., & Feng, W. 2020, The Astrophysical Journal Letters, 905, L11, doi: 10.3847/2041-8213/abcb84

Li, K. J., Xu, J. C., Yin, Z. Q., & Feng, W. 2019, The Astrophysical Journal, 875, 90, doi: 10.3847/1538-4357/ab0f3a

Linsky, J. L., & Avrett, E. H. 1970, Publications of the Astronomical Society of the Pacific, 82, 169, doi: 10.1086/128904

Livingston, W., & Duvall, T. L., J. 1979, SoPh, 61, 219, doi: 10.1007/BF00150407

Livingston, W., Wallace, L., White, O. R., & Giampapa, M. S. 2007, The Astrophysical Journal, 657, 1137, doi: 10.1086/511127

Livingston, W. C. 1969, Solar Physics, 9, 448, doi: 10.1007/BF02391670

Loukitcheva, M., Solanki, S. K., & White, S. M. 2009, Astronomy and Astrophysics, 497, 273, doi: 10.1051/0004-6361/200811133

Malherbe, J.-M. 2023, Journal for the History of Astronomy, doi: 10.1177/00218286231184193

Malherbe, J. M., & Dalmasse, K. 2019, SoPh, 294, 52, doi: 10.1007/s11207-019-1441-7

Markwardt, C. B. 2009, in Astronomical Society of the Pacific Conference Series, Vol. 411, Astronomical Data Analysis Software and Systems XVIII, ed. D. A. Bohlender, D. Durand, & P. Dowler, 251. https://arxiv.org/abs/0902.2850

Murabito, M., Ermolli, I., Chatzistergos, T., et al. 2023, The Astrophysical Journal, 947, 18, doi: 10.3847/1538-4357/acc529

Newton, H. W., & Nunn, M. L. 1951, Monthly Notices of the Royal Astronomical Society, 111, 413, doi: 10.1093/mnras/111.4.413

Paternò, L. 2010, Astrophysics and Space Science, 328, 269, doi: 10.1007/s10509-009-0218-0

Priest, E. 2014, Magnetohydrodynamics of the Sun, doi: 10.1017/CBO9781139020732

Priyal, M., Singh, J., Ravindra, B., Priya, T. G., & Amareswari, K. 2014, SoPh, 289, 137, doi: 10.1007/s11207-013-0315-7

Rodríguez Gómez, J. M., Palacios, J., Vieira, L. E. A., & Dal Lago, A. 2019, ApJ, 884, 88, doi: 10.3847/1538-4357/ab40af

Roša, D., Brajša, R., Vršnak, B., & Wöhl, H. 1995, SoPh, 159, 393, doi: 10.1007/BF00686540

Scherrer, P. H., Bogart, R. S., Bush, R. I., et al. 1995, Solar Physics, 162, 129, doi: 10.1007/BF00733429

Schroeter, E. H., & Woehl, H. 1975, SoPh, 42, 3, doi: 10.1007/BF00153278

Sharma, J., Kumar, B., Malik, A. K., & Vats, H. O. 2020, Monthly Notices of the Royal Astronomical Society, 492, 5391, doi: 10.1093/mnras/staa188

Simon, G. W., & Noyes, R. W. 1972, SoPh, 26, 8, doi: 10.1007/BF00155100

Singh, J., & Prabhu, T. P. 1985, SoPh, 97, 203, doi: 10.1007/BF00152989

Skokić, I., Brajša, R., Roša, D., Hržina, D., & Wöhl, H. 2014, SoPh, 289, 1471, doi: 10.1007/s11207-013-0426-1

Solanki, S. K. 2003, A&A Rv, 11, 153, doi: 10.1007/s00159-003-0018-4

Stix, M. 1976, A&A, 47, 243

Ternullo, M. 1986, Solar Physics, 105, 197, doi: 10.1007/BF00156387

Ternullo, M., Ternullo, & Maurizio. 1987, SoPh, 112, 143, doi: 10.1007/BF00148494

Thompson, W. T. 2006, A&A, 449, 791, doi: 10.1051/0004-6361:20054262

Tlatov, A. G., Pevtsov, A. A., & Singh, J. 2009, SoPh, 255, 239, doi: 10.1007/s11207-009-9326-9

Wan, M., & Gao, P.-x. 2022, The Astrophysical Journal, 939, 111, doi: 10.3847/1538-4357/ac930d

Wan, M., Gao, P. X., Xu, J. C., et al. 2023, Monthly Notices of the Royal Astronomical Society, 520, 988, doi: 10.1093/mnras/stad192

Wan, M., & Li, K. 2022, SoPh, 297, 126, doi: 10.1007/s11207-022-02059-5

Ward, F. 1966, ApJ, 145, 416, doi: 10.1086/148783

Weber, E. J. 1969, SoPh, 9, 150, doi: 10.1007/BF00145735

Wittmann, A. D. 1996, SoPh, 168, 211, doi: 10.1007/BF00145837

Xu, J.-C., Gao, P.-X., & Shi, X.-J. 2020, ApJ, 902, 64, doi: 10.3847/1538-4357/abb5b7

Zhang, X., Deng, L., Fei, Y., Li, C., & Tian, X. 2023, The Astrophysical Journal Letters, 951, L3, doi: 10.3847/2041-8213/ACD9A3

Zirin, H. 1974, Symposium - International Astronomical Union, 56, 161–175, doi: 10.1017/S0074180900069047

APPENDIX

A. THRESHOLD IN CC

In this section, we explain the reason behind our choice of imposing a threshold in CC so as to not bias our results. Since, in our study, we have not pre-selected the best images or the latitude bands where plages are prominently present for our analysis, it may negatively impact our inference as our image correlation method is dominantly affected by the presence of plages and artifacts. In the latitudinal bands, where plages are mostly absent (see B3 and B4 in Figure 8), we see either no/minute variation in CC in the cross-correlation matrix (one such example is shown in Figure 8). There are cases where we see plages, still, we see similar behaviour of CC due to the poor image quality. Therefore, we only select the latitude range where we rarely expect the presence of plages (above $55°$ latitude). In addition to these, to calculate the best chosen Ω values, we have put a lower threshold on CC_{max} of 0.2 in our analysis. In Figure 9, we notice that there is a sudden jump in differential rotation parameter (A) as we switch from 0.1 to 0.2, but no significant variation is seen after we increase the lower threshold from 0.2 to 0.7 in CC_{max} (apart from the change in uncertainty because of poor statistics). Thus, to maximize the statistics and there is no significant change in the results after the CC_{max} threshold value of 0.2, we decided to go with 0.2 as our lower limit on CC_{max}. However, we emphasize that the reasons for low cross-correlation can be physical, such as the absence of plage regions mentioned above, but also technical, such as image distortions or artifacts unaccounted for by the processing techniques or even inaccurate orientation of the images. Restricting our analysis to locations where plage is found would completely miss these technical cases and have the potential to bias our results. The use of a threshold in the cross-correlation is a more robust way not to let such artifacts affect our results.
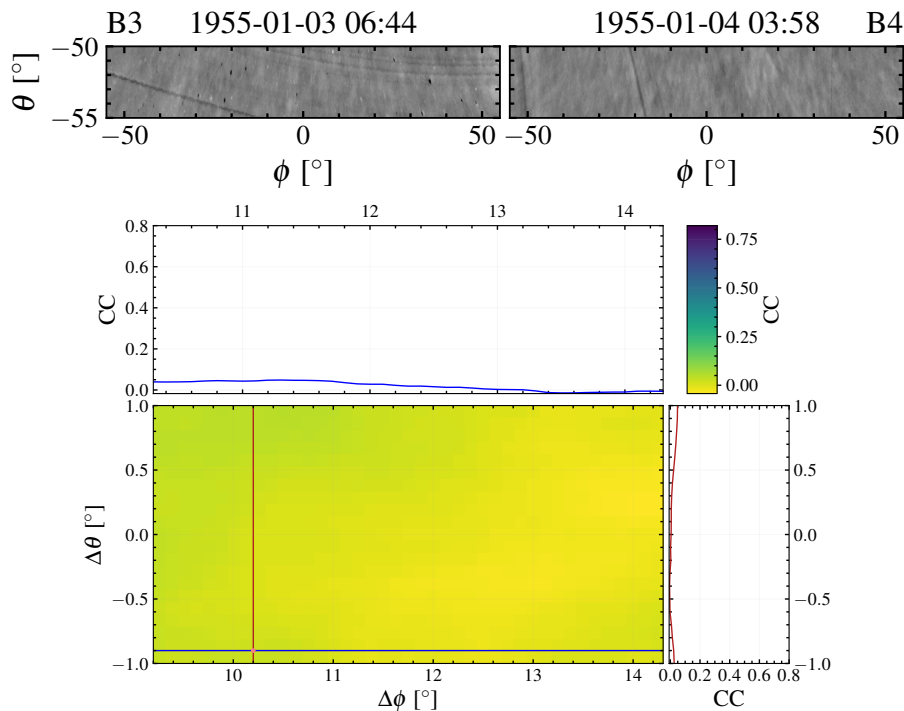

Figure 8. The middle panel shows the 2D cross-correlation profile similar to Figure 2 but for latitudinal bins shown in B3 and B4 (in this case $-55°$ to $-50°$) where plages are absent.

B. METHOD CROSS-VALIDATION USING MDI CONTINUUM INTENSITY AND MWO DATA

The Michelson Doppler Imager (MDI; Scherrer et al. 1995) instrument on the Solar and Heliospheric Observatory (SOHO) satellite has provided a comprehensive dataset of Continuum Intensity (CI) observations spanning 15 years
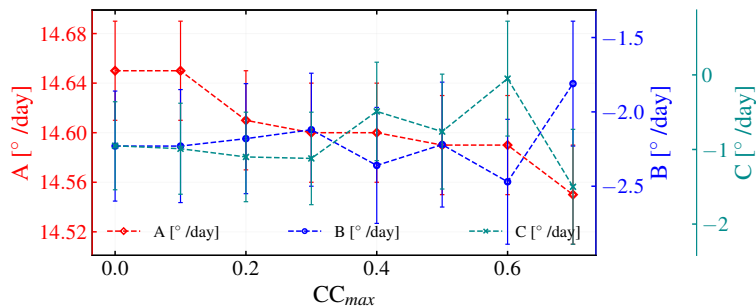
Figure 9. The change in differential rotation parameters by varying CC_{max} threshold.

$(1996-2011)$[4]. In a recent study conducted by Jha et al. (2021), the rotation profile of the solar photosphere was determined through the tracking of sunspots by utilizing MDI CI data. Taking advantage of the pre-established results derived from MDI CI data for the photosphere's rotation profile, we applied our image correlation methodology to verify its consistency. Our analysis, as depicted in Figure 10(a), illustrates an overlap between the rotation profiles obtained via the two approaches (blue square; image correlation and red diamond; sunspot tracking). Furthermore, the scatter plot of angular velocity (Ω) values obtained through these two methods, as presented in (Figure 10(b)), demonstrates a Pearson correlation coefficient of 0.99. This high correlation coefficient serves as compelling evidence substantiating the validity and robustness of our methodology.

Mount Wilson Observatory (MWO) has observed Ca II K images (spectroheliograms; 0.035 nm pass band filter) of the Sun from 1915 to 1985. The study of chromospheric differential rotation was done on MWO Ca II K data (1915–1985) by Bertello et al. (2020) and it was found that the chromosphere rotates slower compared to the photosphere (discussed in section 4). To verify our method, we followed the same procedure as our method for the newly calibrated data done by Chatzistergos et al. (2018, 2019a, 2020) and for the data calibrated by Bertello et al. (2010)[5]. For the data of Bertello et al. (2010), we used the resolution of the heliographic grid as 0.25 instead of 0.1 because the mentioned data have spatial pixels of 866 pixels × 866 pixels. Here, we must note that the data calibrated in Bertello et al. (2010) are further used in Bertello et al. (2020) for the measurement of the MWO rotation rate. Surprisingly, we observed a significant difference in the results obtained from both data, as can be seen in Figure 10(c). The rotation rate acquired from MWO data processed by Chatzistergos et al. (green curve; 2020) is higher than the result by Bertello et al. (brown curve; 2020), and closer to our result for KoSO data (red curve). However, our estimate of differential rotation with MWO analyzed by Bertello et al. (magenta curve; 2010) suggests a slightly slower rotation rate than the result by Bertello et al. (brown curve; 2020) for the same data. Various things contribute to these differences, including the different approaches in preprocessing and calibrating the MWO data, as well as in the process of determining the differential rotation. But what particular step in the preprocessing and calibration is affecting is still not understood. Also, we plotted the scatter plot of both Ω values and got the Pearson correlation coefficient of 0.99 (Chatzistergos et al. 2020) and 0.98 (Bertello et al. 2010) that can be seen in (Figure 10(d)) which shows the strong correlation between KoSO and MWO data set.

---

[4] Data is available at http://jsoc.stanford.edu/

[5] the data are from http://www.astro.ucla.edu/~ulrich/MW_SPADP
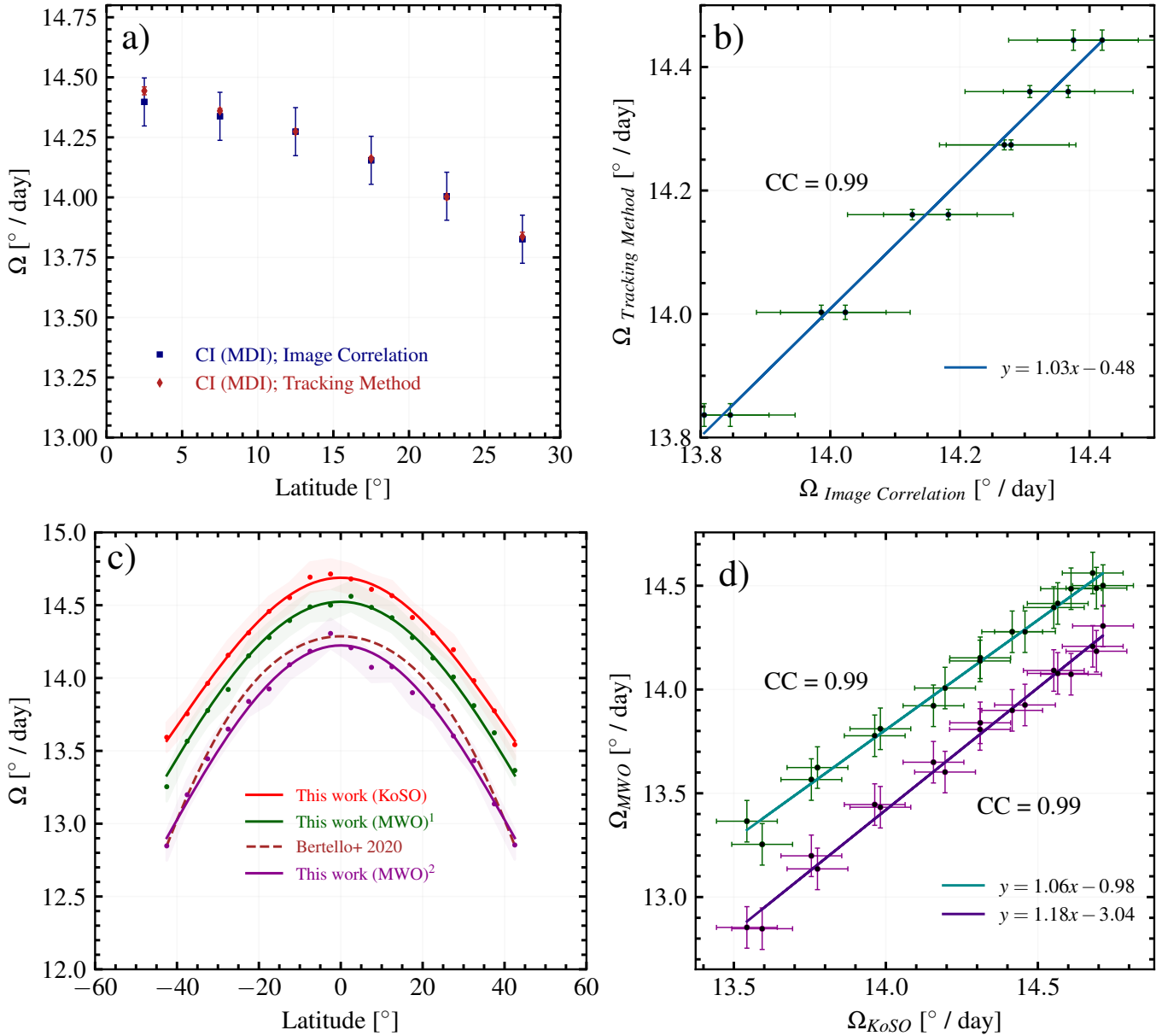
Figure 10. (a) The photospheric rotation profile determined with the feature tracking method on MDI Continuum Intensity (CI) data and with the image cross-correlation technique, respectively. (b) The correlation plot between the angular rotation rate values obtained from the tracking method and the image cross-correlation technique. (c) The rotational profile of the chromosphere using MWO data for the period (1978−1979). The red curve shows the rotational profile for the KoSO Ca II K data (1978−1979), while the green curve and magenta represent the MWO rotation profile using data calibrated by Chatzistergos et al. (2020) and by Bertello et al. (2010). The brown curve represents the results obtained in the past done by Bertello et al. (2020). (d) A correlation plot between the angular rotation rate values obtained from KoSO data and the rotation rate from MWO data.

Note - Chatzistergos et al. (2020)[1], Bertello et al. (2010)[2]